A numerical approximation of the thermal coupling of fluids and solids

Javier Principe*,† and Ramon Codina

CIMNE, Universitat Politècnica de Catalunya, Jordi Girona 1-3, Edifici C1, 08034 Barcelona, Spain

SUMMARY

In this article we analyze the problem of the thermal coupling of fluids and solids through a common interface. We state the global thermal problem in the whole domain, including the fluid part and the solid part. This global thermal problem presents discontinuous physical properties that depend on the solution of auxiliary problems on each part of the domain (a fluid flow problem and a solid state problem). We present a domain decomposition strategy to iteratively solve problems posed in both subdomains and discuss some implementation aspects of the algorithm. This domain decomposition framework is also used to revisit the use of wall function approaches used in this context. Copyright © 2008 John Wiley & Sons, Ltd.

1. INTRODUCTION

The problem we analyze in this article is that of the thermal coupling of fluids and solids. This problem is found in any engineering design in which a fluid is used to extract heat from a solid (refrigeration, ventilation, etc.). In fact, many experimental correlations are available [1] in the form of convection coefficients. The objective of this article is to present a domain decomposition approach that permits the separated treatment of a problem in the solid domain and of a problem in the fluid one. Let us emphasize that it is not our intention to use a domain decomposition strategy to perform parallel computations but to treat problems with different physics separately. Moreover, this domain decomposition approach will allow us to implement the thermal coupling problem in a master–slave algorithm.

The model presented in Section 2 is based on the solution of a thermal problem in the whole domain Ω that includes the solid subdomain Ω_S and the fluid subdomain Ω_F separated by the interface Γ_{SF} which could be, in principle, a moving surface. The differential operators that describe

---

*Correspondence to: Javier Principe, CIMNE, Universitat Politècnica de Catalunya, Jordi Girona 1-3, Edifici C1, 08034 Barcelona, Spain.
†E-mail: principe@cimne.upc.edu

the evolution of the temperature (ϑ) are different as a result of different physics and they depend on other variables that describe the state of each medium. On each subdomain the thermal problem could be coupled to other differential problems depending on the physical model used for the fluid and solid. In the first case we may have a compressible flow or an incompressible one, a mix of species, chemical reactions, etc. In the second case we may have a purely thermal problem, a thermomechanical one or even a thermo-hygro-mechanical one as in [2]. Any model can be used on each subdomain but we will assume that the coupling between the fluid and solid is only due to heat exchange. In the case in which mechanical problems are solved on each subdomain, this assumption is equivalent to assume that

1. the velocities of the solid medium are small and
2. the mechanical traction produced by the fluid on the solid is small.

It will be shown in Section 2 how these conditions result in the uncoupling of the mechanical problems. We will also assume that *the displacements of the solid medium are small enough to consider the interface* Γ_{SF} *fixed*.

The numerical approximation of the fluid and solid problems is in general different. One important feature of our approach is that different numerical approximations could be used to solve each problem. In the case of the fluid we use a stabilized finite element formulation based on the subgrid scale concept. Each field is decomposed into a resolvable and a subgrid scale part according to the finite element partition, and the effect of the subgrid scale on the coarse scale is taken into account by an algebraic approximation. This approach allows us to deal with convection-dominated problems and to use equal-order interpolation of velocity and pressure, which would lead to numerical instabilities when a standard Galerkin formulation is used. The Galerkin approximation is used to solve the solid problem. We describe the discrete formulation in Section 3 but we emphasize once again that any other possibility could be used.

The possibility of using different models and different discrete approximations is not only theoretical but also practical. The coupling through the common interface between the solid and the fluid is accomplished by the transmission conditions, which we consider of Dirichlet/Neumann type. This leads to a non-overlapping domain decomposition problem that we implement in an iteration-by-subdomain strategy. The solution of each thermal problem, in the fluid and in the solid regions, and the transmission of boundary conditions from one domain to the other is done by a relatively small master code. This code, developed following the MPI 2 standard, is in charge of managing the subdomain iterative coupling and the time-marching loops. In this way, each dedicated code acts as a slave and can be updated separately as only minor modifications are needed to change the information with the master code. These implementation aspects are described in Section 4. The domain decomposition framework for the thermal coupling described, together with its implementation aspects and an interpretation of the use of wall function approaches, is the main contribution of this work.

Finally, the approach is illustrated in a simple one-dimensional example and is applied to the simulation of a fire in a tunnel in Section 5. Some conclusions are drawn in Section 6.

2. CONTINUOUS PROBLEM

We consider a thermal problem in a domain Ω composed of two subdomains Ω_S and Ω_F, as illustrated in Figure 1 (left and center). First, we present the problem in the whole domain considering
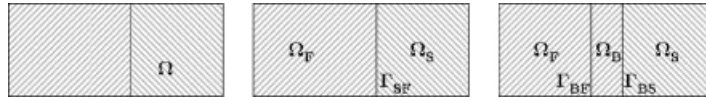
Figure 1. Domain of the problem.

discontinuous physical properties, which include the density (ρ), the specific heat (c_p) and the diffusion coefficient ($\kappa = k/\rho c_p$, where k is the thermal conductivity), as well as a velocity field (**v**). This velocity field will be assumed to be solution of a mechanical problem defined also in the whole domain and having also discontinuous properties. The constitutive relations in the fluid and in the solid are different, the former relating the stress tensor ($\boldsymbol{\sigma}$) to the velocity gradients and the latter relating the stress tensor to the deformation gradient.

Once the problem in the whole domain has been expressed, we will present two different strategies for a domain decomposition approach to this problem. The first strategy presented consists of a standard non-overlapping domain decomposition of the problem into the fluid and solid subdomains. We will assume that the mechanical problem in the solid does not depend on that in the fluid, in a sense to be made precise later on. We will refer to this approach as *the full resolution strategy*.

The second strategy consists of a non-overlapping domain decomposition of the problem in three subdomains, one in the solid region and two in the fluid region, as illustrated in Figure 1 (right). One of the fluid subdomains will be a thin region of thickness δ near the solid surface and the other will be the rest of the fluid domain. The purpose of this second approach is to consider the problem of the strong boundary layers present in a turbulent flow using the wall function approach. An approximated solution of the problem in this thin region is expressed in terms of the wall function and an iteration strategy between the remaining subdomains is proposed. Therefore, this second approach will also involve two subdomains. We again assume that the mechanical problems are uncoupled. We will refer to this approach as the *wall function strategy*.

2.1. Problem definition in the whole domain

2.1.1. Strong form of the problem. The problem to be solved in Ω, an open domain in $\mathbb{R}^d$ ($d = 2, 3$ is the number of space dimensions) during the time interval $(0, t_f)$ is described by the equations of continuous media. Although a complex model can be used [2] the set of equations always contain an energy conservation statement that, under suitable assumptions, reads

$$\rho c_p (\partial_t \vartheta + \mathbf{v} \cdot \nabla \vartheta) + \nabla \cdot \mathbf{q} = Q \quad \text{in } \Omega \times (0, t_f) \tag{1}$$

where Q is the external source of energy source per unit of mass and **q** is the internal heat flux vector. The velocity field **v** is the solution of a mechanical problem of the form

$$\rho (\partial_t \mathbf{v} + \mathbf{v} \cdot \nabla \mathbf{v}) - \nabla \cdot \boldsymbol{\sigma} = \rho \mathbf{g} \quad \text{in } \Omega \times (0, t_f)$$

where **g** is the external source of momentum per unit of mass and $\boldsymbol{\sigma}$ the internal stress tensor. The parameters present in these equations (ρ and c_p) may be discontinuous across the surface Γ_{SF}. The constitutive equation for the internal heat flux is

$$\mathbf{q} = -k \nabla \vartheta \tag{2}$$

where k may also be discontinuous across Γ_{SF}. The constitutive equation for the internal stress tensor will in general be different in both regions. In the case of the solid it will be related to the deformation tensor. In the case of an incompressible fluid it will be related to the velocity gradient and to another variable, the pressure (p), that will involve the solution of another equation, the conservation of mass. The problem must be supplemented with appropriate boundary and initial conditions, which can be expressed as

$$\vartheta = \vartheta_0 \quad \text{in } \Omega \times \{0\}$$

$$\vartheta = \vartheta_D \quad \text{on } \Gamma_D^\vartheta \times (0, t_f)$$

$$\mathbf{n} \cdot \mathbf{q} = q_N \quad \text{on } \Gamma_N^\vartheta \times (0, t_f)$$

where Γ_D^ϑ (Γ_N^ϑ) represent the part of the domain boundary where Dirichlet (Neumann) boundary conditions for the temperature are prescribed, $\partial\Omega = \Gamma_D^\vartheta \cup \Gamma_N^\vartheta$ and $\mathbf{n}$ is the exterior normal to the domain Ω. In turn, the initial and boundary conditions for the mechanical problem depend on the constitutive relation considered. In the case of a solid, they are usually expressed in terms of the displacement and in the case of the fluid in terms of the velocity. The purpose of expressing the mechanical problem is to clearly specify the conditions under which it is uncoupled. Nevertheless, we will consider the weak form and the numerical approximation of the thermal problem only.

2.1.2. Weak form of the problem. As usual we denote by $H^1(\Omega)$ the space of functions whose first-order derivatives belong to $L^2(\Omega)$, the space of square-integrable functions in Ω, by $\langle u, v \rangle_\omega = \int_\omega u v$ and by $(u, v)_\Omega$ the scalar product in $L^2(\Omega)$. The space of $H^1(\Omega)$ functions that satisfy Dirichlet boundary conditions will be denoted by V^ϑ (V^0 for zero Dirichlet boundary conditions). The weak form of the problem consists in finding $\vartheta \in L^2(0, t_f; V^\vartheta) \cap L^\infty(0, t_f; L^2(\Omega))$ such that

$$a(\vartheta, v) = l(v) \quad \forall v \in V^0 \tag{3}$$

where $L^2(0, t_f; V^\vartheta)$ is the set of functions whose norm in V^ϑ (which is the norm in $H^1(\Omega)$) is square integrable in time, and $L^\infty(0, t_f; L^2(\Omega))$ the set of functions whose norm in $L^2(\Omega)$ is bounded in time. The bilinear form a and the linear form l are defined as

$$a(\vartheta, v) := (\rho c_p \partial_t \vartheta, v)_\Omega + (\rho c_p \mathbf{v} \cdot \nabla \vartheta, v)_\Omega + (k \nabla \vartheta, \nabla v)_\Omega$$

and

$$l(v) := \langle Q, v \rangle_\Omega + \langle q_N, v \rangle_{\Gamma_N^\vartheta}$$

respectively (in fact, a is affine in the first argument, but we will omit this precision in the following).

2.2. The full resolution strategy

A standard non-overlapping domain decomposition of the problem is obtained by splitting the domain Ω into the solid and fluid subdomains, Ω_S and Ω_F, as illustrated in Figure 1 (center), where the notation that we will use is indicated.

2.2.1. Strong form of the problem. The strong form of the problem consists in finding temperatures ϑ_S and ϑ_F, as well as velocities $\mathbf{v}_F$ (in the fluid) and displacements $\mathbf{u}_S$ (in the solid), such that

$$\rho_S c_{pS} \partial_t \vartheta_S + \nabla \cdot \mathbf{q}_S = Q_S \quad \text{in } \Omega_S \times (0, t_f)$$

$$-\nabla \cdot \boldsymbol{\sigma}_S = \rho \mathbf{g} \quad \text{in } \Omega_S \times (0, t_f)$$

and

$$\rho_F c_{pF}(\partial_t \vartheta_F + \mathbf{v}_F \cdot \nabla \vartheta_F) + \nabla \cdot \mathbf{q}_F = Q_F \quad \text{in } \Omega_F \times (0, t_f)$$

$$\rho_F(\partial_t \mathbf{v}_F + \mathbf{v}_F \cdot \nabla \mathbf{v}_F) - \nabla \cdot \boldsymbol{\sigma}_F = \rho \mathbf{g} \quad \text{in } \Omega_F \times (0, t_f)$$

Here we have used Assumption 1 of Section 1 to neglect the terms containing the velocity of the solid. For the sake of simplicity in the exposition, accelerations have also been neglected (quasi-static problem). The conditions to be satisfied at the interface are the continuity of the temperatures and velocities as well as the normal components of heat fluxes and tractions that read

$$\mathbf{v}_F|_{\Gamma_{SF}} = \mathbf{v}_S|_{\Gamma_{SF}} = \dot{\mathbf{u}}_S|_{\Gamma_{SF}}$$

$$\mathbf{n}_F \cdot \boldsymbol{\sigma}_F|_{\Gamma_{SF}} = -\mathbf{n}_S \cdot \boldsymbol{\sigma}_S|_{\Gamma_{SF}}$$

and

$$\vartheta_F|_{\Gamma_{SF}} = \vartheta_S|_{\Gamma_{SF}}$$

$$\mathbf{n}_F \cdot \mathbf{q}_F|_{\Gamma_{SF}} = -\mathbf{n}_S \cdot \mathbf{q}_S|_{\Gamma_{SF}}$$

where now $\mathbf{n}_S$ ($\mathbf{n}_F$) is the normal exterior to the domain Ω_S (Ω_F). At this point Assumptions 1 and 2 of Section 1 yield $\dot{\mathbf{u}}_S \approx \mathbf{0}$ and $\mathbf{n}_F \cdot \boldsymbol{\sigma}_F|_{\Gamma_{SF}} \approx \mathbf{0}$, respectively. With these approximations the interface conditions become

$$\mathbf{v}_F|_{\Gamma_{SF}} = \mathbf{0}$$

$$\mathbf{n}_S \cdot \boldsymbol{\sigma}_S|_{\Gamma_{SF}} = \mathbf{0}$$

and

$$\vartheta_F|_{\Gamma_{SF}} = \vartheta_S|_{\Gamma_{SF}}$$

$$\mathbf{n}_F \cdot \mathbf{q}_F|_{\Gamma_{SF}} = -\mathbf{n}_S \cdot \mathbf{q}_S|_{\Gamma_{SF}}$$

and therefore the mechanical problems are uncoupled.

2.2.2. Weak form of the problem. Let us introduce the bilinear forms a_S defined on the solid subdomain Ω_S as

$$a_S(\vartheta, v) := (\rho_S c_{pS} \partial_t \vartheta_S, v)_{\Omega_S} + (k_S \nabla \vartheta_S, \nabla v)_{\Omega_S}$$

and on the fluid subdomain Ω_F as

$$a_F(\vartheta, v) := (\rho_F c_{pF} \partial_t \vartheta_F, v)_{\Omega_F} + (\rho_F c_{pF} \mathbf{v}_F \cdot \nabla \vartheta_F, v)_{\Omega_F} + (k_F \nabla \vartheta_F, \nabla v)_{\Omega_F}$$

We also introduce the linear forms

$$l_S(v) := \langle Q_S, v \rangle_{\Omega_S} + \langle q_N, v \rangle_{\Gamma_{NS}^\vartheta}$$

and

$$l_F(v) := \langle Q_F, v \rangle_{\Omega_F} + \langle q_N, v \rangle_{\Gamma_{NF}^\vartheta}$$

The weak form of the problem consists in finding

$$\vartheta_S \in L^2(0, t_f; V_S^\vartheta) \cap L^\infty(0, t_f; L^2(\Omega_S))$$

$$\vartheta_F \in L^2(0, t_f; V_F^\vartheta) \cap L^\infty(0, t_f; L^2(\Omega_F))$$

such that

$$
\begin{aligned}
a_S(\vartheta, v) - \langle k_S \mathbf{n}_S \cdot \nabla \vartheta_S, v \rangle_{\Gamma_{SF}} &= l_S(v) \quad \forall v \in V_S^0 \\
a_F(\vartheta, v) - \langle k_F \mathbf{n}_F \cdot \nabla \vartheta_F, v \rangle_{\Gamma_{SF}} &= l_F(v) \quad \forall v \in V_F^0 \\
\vartheta_F &= \vartheta_S \quad \text{on } \Gamma_{SF} \\
k_F \mathbf{n}_F \cdot \nabla \vartheta_F |_{\Gamma_{SF}} &= -k_S \mathbf{n}_S \cdot \nabla \vartheta_S |_{\Gamma_{SF}} \quad \text{on } \Gamma_{SF}
\end{aligned}
\tag{4}
$$

where the spaces V_S^ϑ and V_S^0 (respectively, V_F^ϑ and V_F^0) are defined in the same manner as V^ϑ and V^0 but considering Γ_{DS}^ϑ (respectively, Γ_{DF}^ϑ) instead of Γ_D^ϑ.

2.3. The wall function strategy

Now we use again a standard non-overlapping domain decomposition of the problem but splitting the domain Ω into the solid subdomain Ω_S, a boundary layer in the fluid Ω_B and the rest of the fluid subdomain Ω_F, as illustrated in Figure 1 (right). In addition, let Γ_{SB} be the interface between Ω_S and Ω_B, and Γ_{BF} be the interface between Ω_B and Ω_F. Apart from the equations given in the previous subsection for the solid and the fluid subdomains, we now need to solve the problem on the boundary layer subdomain, which consists in finding a temperature ϑ_B and a velocity $\mathbf{v}_B$ such that

$$\rho c_p(\partial_t \vartheta_B + \mathbf{v}_B \cdot \nabla \vartheta_B) + \nabla \cdot \mathbf{q}_B = Q_B \tag{5}$$

$$\rho(\partial_t \mathbf{v}_B + \mathbf{v}_B \cdot \nabla \mathbf{v}_B) - \nabla \cdot \boldsymbol{\sigma}_B = \rho \mathbf{g} \tag{6}$$

Under the same assumptions as in the previous subsection the interface conditions are

$$\mathbf{v}_B |_{\Gamma_{SB}} = \mathbf{0}$$

$$\mathbf{n}_S \cdot \boldsymbol{\sigma}_S |_{\Gamma_{SB}} = \mathbf{0}$$

$$\vartheta_B |_{\Gamma_{SB}} = \vartheta_S |_{\Gamma_{SB}}$$

$$\mathbf{n}_B \cdot \mathbf{q}_B |_{\Gamma_{SB}} = -\mathbf{n}_S \cdot \mathbf{q}_S |_{\Gamma_{SB}}$$

and

$$\mathbf{v}_F|_{\Gamma_{BF}} = \mathbf{v}_B|_{\Gamma_{BF}}$$

$$\mathbf{n}_F \cdot \boldsymbol{\sigma}_F|_{\Gamma_{BF}} = -\mathbf{n}_B \cdot \boldsymbol{\sigma}_B|_{\Gamma_{BF}}$$

$$\vartheta_F|_{\Gamma_{BF}} = \vartheta_B|_{\Gamma_{BF}}$$

$$\mathbf{n}_F \cdot \mathbf{q}_F|_{\Gamma_{BF}} = -\mathbf{n}_B \cdot \mathbf{q}_B|_{\Gamma_{BF}}$$

If the boundary layer is of constant width, one may assume that its normal satisfies

$$\mathbf{n}_B|_{\Gamma_{SB}} = -\mathbf{n}_B|_{\Gamma_{BF}}$$

The problem on the boundary layer subdomain is now approximately solved using the wall function approach, which is described next.

2.3.1. Wall function revisited. The so-called wall function approach is a method for the approximate solution of the fluid mechanics problems with strong boundary layers. These boundary layers are removed from the computational domain and universal velocity profiles are used to define the boundary condition in terms of the boundary conditions on the solid surface, as shown in Figure 2. This approximated solution is found assuming negligible inertial terms and external forces. From (5) and (6) it is seen that this yields

$$\nabla \cdot \mathbf{q}_B = 0$$

$$\nabla \cdot \boldsymbol{\sigma}_B = 0$$

which imply constant stresses and heat fluxes across the boundary layer. Now, we denote as q the normal component of the heat flux

$$q = \mathbf{n}_B \cdot \mathbf{q}_B|_{\Gamma_{SB}}$$

and as $\mathbf{t}$ the tangential stress

$$\mathbf{t} = \mathbf{n} \cdot \boldsymbol{\sigma}_B - (\mathbf{n} \cdot \boldsymbol{\sigma}_B \cdot \mathbf{n})\mathbf{n}|_{\Gamma_{SB}}$$
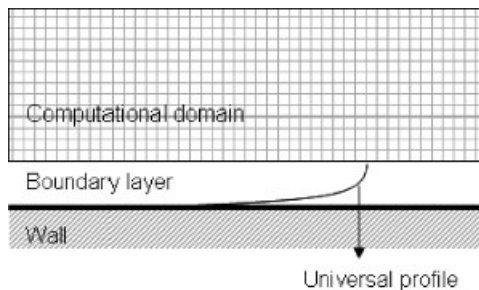

Figure 2. A wall function approach.

evaluated at the wall. The mechanical problem is solved selecting a local coordinate system such that the first local direction is **t**. If we denote by σ the norm of the tangential component of the stress (not to be confused with the full stress tensor), by u_B the component of the velocity in this system and by y the coordinate normal to the solid surface, the constitutive equations are

$$q = (k + k^t) \frac{d\vartheta_B}{dy} \tag{7}$$

$$\sigma = (\mu + \mu^t) \frac{du_B}{dy} \tag{8}$$

where μ^t and k^t are the turbulent viscosity and conductivity. Given the turbulent viscosity and conductivity we can integrate (7) and (8) to obtain the velocity and temperature profiles. The definition of the turbulent viscosity and conductivity is the definition of the model we are using to approximate the problem and is based on experimental correlations [3]. One of these models is the one that results in the logarithmic profiles for the velocity and temperature. This model is based on the existence of a zone near the wall, called laminar sublayer, in which the velocity is small and as well the local Reynolds number. In the laminar sublayer the turbulent viscosity is neglected and we have

$$\sigma = \mu \frac{du_B}{dy}$$

that is expressed in the dimensionless form introducing the friction velocity $u_* = \sqrt{\sigma|_{y=0}/\rho}$. As the stress is constant across the boundary layer, we have

$$\frac{u_B}{u_*} = \frac{\rho u_* y}{\mu}$$

On the other hand, in the turbulent region we may approximate $\mu^t = \rho \kappa y u_*$, κ being the Von Karman constant, and integrating (8) we have

$$\frac{u_B}{u_*} = \frac{u_0}{u_*} + \frac{1}{\kappa} \ln\left(\frac{y}{y_0}\right)$$

where y_0 is the width of the laminar sublayer and u_0 the value of the velocity at this point. Defining the dimensionless velocity $u_B^+ = u_B/u_*$ and distance $y^+ = \rho y u^*/\mu$ and taking $y_0^+ = 11.6$ the final solution reads

$$u_B^+ = \begin{cases} y^+ & \text{if } y^+ < y_0^+ \\ \dfrac{1}{\kappa} \ln(y^+) + 5.5 & \text{if } y^+ \geqslant y_0^+ \end{cases}$$

In the same manner, integrating (7) we arrive at

$$\vartheta_B^+ = \begin{cases} Pr\, y^+ & \text{if } y^+ < y_0^+ \\ Pr^t \left[\dfrac{1}{\kappa} \ln(y^+) + P_\theta \right] & \text{if } y^+ \geqslant y_0^+ \end{cases}$$

where $Pr := \rho\kappa/\mu$ is the Prandtl number, Pr^{t} is the turbulent Prandtl number (which is part of the constitutive model), P_θ a function that gives the temperature jump across the laminar sublayer and the dimensionless temperature is defined as

$$\vartheta_{\mathrm{B}}^+ = -\frac{\rho c_p u_*}{q}(\vartheta - \vartheta_{\mathrm{B}}|_{\Gamma_{\mathrm{SB}}})$$

2.3.2. Strong form of the problem. Having an analytical solution to the problem in the boundary layer domain we can rewrite the complete problem in terms of two subdomains, the fluid (excluding the boundary layer) and the solid. To this end, let us remark that the solution of the thermal problem obtained using the wall function method is a constant heat flux and therefore

$$q = \mathbf{n}_{\mathrm{S}} \cdot \mathbf{q}_{\mathrm{S}}|_{\Gamma_{\mathrm{SB}}} = -\mathbf{n}_{\mathrm{B}} \cdot \mathbf{q}_{\mathrm{B}}|_{\Gamma_{\mathrm{SB}}} = \mathbf{n}_{\mathrm{B}} \cdot \mathbf{q}_{\mathrm{B}}|_{\Gamma_{\mathrm{BF}}} = -\mathbf{n}_{\mathrm{F}} \cdot \mathbf{q}_{\mathrm{F}}|_{\Gamma_{\mathrm{BF}}}$$

This flux is proportional to the temperature jump across the layer

$$q = \alpha(\vartheta_{\mathrm{B}}|_{\Gamma_{\mathrm{BF}}} - \vartheta_{\mathrm{B}}|_{\Gamma_{\mathrm{SB}}}) = \alpha(\vartheta_{\mathrm{F}}|_{\Gamma_{\mathrm{BF}}} - \vartheta_{\mathrm{S}}|_{\Gamma_{\mathrm{SB}}})$$

where

$$\alpha = \frac{\rho c_p u_*}{\vartheta^+}$$

and $\vartheta^+ = \vartheta_{\mathrm{B}}^+(\delta^+)$ is defined in terms of δ^+, the dimensionless boundary layer thickness. This parameter depends, finally, on the particular choice of the turbulent viscosity and conductivity of the wall function method. In the same manner, as the tangential stress is constant across the boundary layer, we have

$$\mathbf{t}|_{\Gamma_{\mathrm{SB}}} = \mathbf{t}|_{\Gamma_{\mathrm{BF}}} = \beta \mathbf{v}_{\mathrm{F}}|_{\Gamma_{\mathrm{BF}}}$$

for a certain parameter β, and the normal component of the velocity is set to zero

$$\mathbf{n} \cdot \mathbf{v}_{\mathrm{F}}|_{\Gamma_{\mathrm{BF}}} = 0$$

We can finally state the strong form of the problem as finding ϑ_{S} and ϑ_{F}, as well as $\mathbf{u}_{\mathrm{S}}$ and $\mathbf{v}_{\mathrm{F}}$, such that

$$\rho_{\mathrm{S}} c_{p\mathrm{S}} \partial_t \vartheta_{\mathrm{S}} + \nabla \cdot \mathbf{q}_{\mathrm{S}} = Q_{\mathrm{S}} \quad \text{in } \Omega_{\mathrm{S}} \times (0, t_{\mathrm{f}})$$

$$-\nabla \cdot \boldsymbol{\sigma}_{\mathrm{S}} = \rho \mathbf{g} \quad \text{in } \Omega_{\mathrm{S}} \times (0, t_{\mathrm{f}})$$

and

$$\rho_{\mathrm{S}} c_{p\mathrm{S}}(\partial_t \vartheta_{\mathrm{F}} + \mathbf{v}_{\mathrm{F}} \cdot \nabla \vartheta_{\mathrm{F}}) + \nabla \cdot \mathbf{q}_{\mathrm{F}} = Q_{\mathrm{F}} \quad \text{in } \Omega_{\mathrm{F}} \times (0, t_{\mathrm{f}})$$

$$\rho_{\mathrm{S}}(\partial_t \mathbf{v}_{\mathrm{F}} + \mathbf{v}_{\mathrm{F}} \cdot \nabla \mathbf{v}_{\mathrm{F}}) - \nabla \cdot \boldsymbol{\sigma}_{\mathrm{F}} = \rho \mathbf{g} \quad \text{in } \Omega_{\mathrm{F}} \times (0, t_{\mathrm{f}})$$

and now the interface conditions become

$$\mathbf{t}|_{\Gamma_{\mathrm{BF}}} = \beta \mathbf{v}_{\mathrm{F}}|_{\Gamma_{\mathrm{BF}}}$$

$$\mathbf{n}_{\mathrm{F}} \cdot \mathbf{v}_{\mathrm{F}}|_{\Gamma_{\mathrm{BF}}} = 0$$

$$\mathbf{n}_{\mathrm{S}} \cdot \boldsymbol{\sigma}_{\mathrm{S}}|_{\Gamma_{\mathrm{SB}}} = \mathbf{0}$$

and

$$q = \mathbf{n}_S \cdot \mathbf{q}_S|_{\Gamma_{SB}} = -\mathbf{n}_B \cdot \mathbf{q}_B|_{\Gamma_{SB}} = \mathbf{n}_B \cdot \mathbf{q}_B|_{\Gamma_{BF}} = -\mathbf{n}_F \cdot \mathbf{q}_F|_{\Gamma_{BF}}$$

$$= \alpha(\vartheta_B|_{\Gamma_{BF}} - \vartheta_B|_{\Gamma_{SB}}) = \alpha(\vartheta_F|_{\Gamma_{BF}} - \vartheta_S|_{\Gamma_{SB}})$$

Finally, assuming the boundary layer to be thin, we can express the final approximation as

$$q = \mathbf{n}_S \cdot \mathbf{q}_S|_{\Gamma_{SF}} = -\mathbf{n}_F \cdot \mathbf{q}_F|_{\Gamma_{SF}}$$

$$= \alpha(\vartheta_F|_{\Gamma_{SF}} - \vartheta_S|_{\Gamma_{SF}})$$

which is a surface-convection-type boundary condition. As in [4], we have derived an expression for α based on the physical model being used (with a completely different meaning with respect to the mentioned reference).

2.3.3. Weak form of the problem. Using the notation of the previous subsection, the weak form of the problem consists in finding

$$\vartheta_S \in L^2(0, t_f; V_S^\vartheta) \cap L^\infty(0, t_f; L^2(\Omega_S))$$

$$\vartheta_F \in L^2(0, t_f; V_F^\vartheta) \cap L^\infty(0, t_f; L^2(\Omega_F))$$

such that

$$a_S(\vartheta, v) - \langle k_S \mathbf{n}_S \cdot \nabla \vartheta_S, v \rangle_{\Gamma_{SF}} = l(v) \quad \forall v \in V_S^0$$

$$a_F(\vartheta, v) - \langle k_F \mathbf{n}_F \cdot \nabla \vartheta_F, v \rangle_{\Gamma_{SF}} = l(v) \quad \forall v \in V_F^0$$

$$k_F \mathbf{n}_F \cdot \nabla \vartheta_F|_{\Gamma_{SF}} = \alpha(\vartheta_F|_{\Gamma_{SF}} - \vartheta_S|_{\Gamma_{SF}}) \quad \text{on } \Gamma_{SF}$$

$$k_F \mathbf{n}_F \cdot \nabla \vartheta_F|_{\Gamma_{SF}} = -k_S \mathbf{n}_S \cdot \nabla \vartheta_S|_{\Gamma_{SF}} \quad \text{on } \Gamma_{SF}$$

Comparing the weak form of this problem to (4) the only difference is a jump on the temperature proportional to the heat flux between domains. Our derivation allows us to give *an interpretation to the surface convection coefficient α in terms of the wall function model* used on the boundary layer subdomain.

3. NUMERICAL APPROXIMATION

Three different continuous problems have been described in Section 2 but the first one, that consists of the solution of a global problem in the whole domain, was presented to define the problem we are facing and has not been actually implemented. The other two possibilities imply the solution of local thermal problems as well as local mechanical problems for the fluid and the solid. In this section we present the numerical approximation to the problem and we will concentrate on the thermal problem only. In the first subsection we will present the finite element discretization of the problem considering generically the domain Ω. This approximation could be applied on the whole domain but will be actually applied on each subdomain. A similar scheme is used to solve the mechanical problem on the fluid. Details on the finite element approximation to the Navier–Stokes equation can be found in [5–7]. In the second subsection we describe an iterative strategy to solve the global thermal problem iteratively solving local problems on each subdomain.

3.1. Finite element approximation

The Galerkin finite element approximation of this problem is standard. Based on a partition of the domain $\mathcal{P}_h = \{K\}$ in n_{el} elements K, the space V^{ϑ} where the temperature is sought is approximated by a finite-dimensional space V_h^{ϑ} (built using polynomials). If the space of test functions V^0 is approximated by V_h^0, defined in a similar manner, the semi-discrete problem consists in finding $\vartheta_h \in L^2(0, t_f; V_h^{\vartheta})$ such that

$$a(\vartheta_h, v_h) = l(v_h) \quad \forall v_h \in V_h^0$$

It is well known that this formulation is unstable when the convection dominates and therefore we employ a stabilized finite element formulation based on the subgrid scale method with an algebraic approximation to the subscales [8]. Details of the formulation are given in [6]. Only the final discrete problem will be presented here.

The time discretization of the problem will be performed using the generalized trapezoidal rule, that is to say, a finite difference scheme. Let us consider a uniform partition of the time interval $(0, t_f)$ of size δt and let us introduce the following notation:

$$f^{n+\theta} = \theta f^{n+1} + (1-\theta) f^n$$

$$\delta_t f^n = (f^{n+1} - f^n)/\delta t = (f^{n+\theta} - f^n)/(\theta \delta t)$$

where $0 < \theta \leqslant 1$. For $\theta = 1$ we obtain the backward Euler scheme of first order, and for $\theta = \frac{1}{2}$ the Crank–Nicolson scheme of second order. Both are unconditionally stable. Let us define

$$a^h(\vartheta_h^{n+1}, v_h) = (\rho^{n+\theta} c_p^{n+\theta} \delta_t \vartheta_h^n, v)_{\Omega} + (\rho^{n+\theta} c_p^{n+\theta} \mathbf{v}^{n+\theta} \cdot \nabla \vartheta_h^{n+\theta}, v)_{\Omega} + (k^{n+\theta} \nabla \vartheta_h^{n+\theta}, \nabla v_h)_{\Omega}$$

$$+ (\rho^{n+\theta} c_p^{n+\theta} \delta_t \widetilde{\vartheta}^n, v_h)_{\Omega} - \sum_K (\rho^{n+\theta} c_p^{n+\theta} \mathbf{v}^{n+\theta} \cdot \nabla v_h + k^{n+\theta} \nabla^2 v_h, \widetilde{\vartheta}^{n+\theta})_K$$

where $\widetilde{\vartheta}^{n+1}$ is given by (see [6] for details)

- quasi-static subscales:

$$\widetilde{\vartheta}^{n+\theta} \approx \tau^{n+\theta} R_h^{n+\theta}$$

- dynamic subscales:

$$\rho^{n+\theta} c_p^{n+\theta} \delta_t \widetilde{\vartheta}^n + \tau^{-1} \widetilde{\vartheta}^{n+\theta} = R_h^{n+\theta}$$

The parameter τ appearing in these expressions is given by

$$\tau = \left[c_1 \frac{k}{h^2} + c_2 \frac{\rho c_p \|\mathbf{v}\|}{h} \right]^{-1}$$

The fully discrete problem consists of: For $n = 1, 2, \ldots$, find $\vartheta_h^{n+1} \in V_h^{\vartheta}$ such that

$$a^h(\vartheta_h^{n+1}, v_h) = \langle q^{n+\theta}, v_h \rangle_{\Omega} + \langle q_N^{n+\theta}, v_h \rangle_{\Gamma_N^{\vartheta}} \quad \forall v_h \in V_h^0$$

3.2. *Coupling strategy*

As mentioned before, we consider a geometric domain decomposition of the problem by means of a non-overlapping subdomain approach. Therefore, at each time step, we expect to construct the solution of the problem from the solution of local problems for the fluid and the structure using the interface conditions already described. This is carried out by iteratively solving local problems on each domain until convergence on the interface conditions is satisfied, that is to say, we use an iteration-by-subdomain strategy [9]. The choice of the boundary conditions of the local problems should be such that the interface conditions presented in Section 2 are satisfied when convergence is achieved. It is well known from the theory of domain decomposition methods that in the case of non-overlapping subdomains we can choose Dirichlet–Neumann (Robin), Neumann (Robin)–Dirichlet or Robin–Robin. Let us define a_S^h and a_F^h in the same manner as a^h was defined in the previous subsection.

If we use the full resolution strategy and apply Dirichlet boundary conditions to the solid and Neumann boundary conditions to the fluid, which according to Giles and Roe *et al.* [10, 11] is the most stable option, the coupling algorithm can be expressed as: For each time step n and each iteration i find $\vartheta_{S,h}^{n+1,i+1} \in V_{S,h}^{\vartheta}$ and $\vartheta_{F,h}^{n+1,i+1} \in V_{F,h}^{\vartheta}$ such that

$$a_S^h(\vartheta_{S,h}^{n+1,i+1}, v_h) = \langle Q^{n+\theta}, v_h \rangle_\Omega + \langle q_N^{n+\theta}, v_h \rangle_{\Gamma_N^{\vartheta}} \tag{9}$$

$$a_F^h(\vartheta_{F,h}^{n+1,i+1}, v_h) = \langle Q^{n+\theta}, v_h \rangle_\Omega + \langle q_N^{n+\theta}, v_h \rangle_{\Gamma_N^{\vartheta}} - \langle k_S \mathbf{n}_S \cdot \nabla \vartheta_{S,h}^{n+1,i}, v_h \rangle_{\Gamma_{SF}} \tag{10}$$

where $v_h \in V_{S,h}^0$ in (9) and in $v_h \in V_{F,h}^0$ in (10). Now it is understood that these spaces, $V_{S,h}^0$ and $V_{S,h}^{\vartheta}$, are constructed including Γ_{SF} in the Dirichlet part of the boundary in order to satisfy

$$\vartheta_{S,h}^{n+1,i+1} = \vartheta_{F,h}^{n+1,k} \quad \text{on } \Gamma_{SF}$$

We can take $k=i+1$ or $k=i$. In the first case, the solution of this problem is sequential, that is, we solve first for the fluid and then for the solid, whereas in the second one it can be parallel.

If we use the wall function strategy, the coupling algorithm can be expressed as: For each time step and each iteration i find $\vartheta_{S,h}^{n+1,i+1} \in V_{S,h}^{\vartheta}$ and $\vartheta_{F,h}^{n+1,i+1} \in V_{F,h}^{\vartheta}$ such that

$$a_S^h(\vartheta_{S,h}^{n+1,i+1}, v_h) = \langle Q^{n+\theta}, v_h \rangle_\Omega + \langle q_N^{n+\theta}, v_h \rangle_{\Gamma_N^{\vartheta}} + \langle \alpha(\vartheta_{S,h}^{n+1,i+1} - \vartheta_{F,h}^{n+1,i}), v_h \rangle_{\Gamma_{SF}} \tag{11}$$

$$a_F^h(\vartheta_{F,h}^{n+1,i+1}, v_h) = \langle Q^{n+\theta}, v_h \rangle_\Omega + \langle q_N^{n+\theta}, v_h \rangle_{\Gamma_N^{\vartheta}} + \langle \alpha(\vartheta_{F,h}^{n+1,i+1} - \vartheta_{S,h}^{n+1,k}), v_h \rangle_{\Gamma_{SF}} \tag{12}$$

where $v_h \in V_{S,h}^0$ in (11) and in $v_h \in V_{F,h}^0$ in (12). Again we can take $k=i+1$ or $k=i$.

Apart from the fact that the physical models represented by Systems (9)–(10) and (11)–(12) are different, some conceptual differences have to be remarked. First, it is observed that the imposition of the transmission conditions is 'symmetric' for the fluid and the solid, contrary to the Dirichlet–Neumann conditions in (9)–(10). Secondly, (11)–(12) does not require the calculation of the normal heat fluxes from the solid to the fluid, as needed in (10). This calculation is always involved in a finite element code, particularly for non-matching meshes between the fluid and the solid (see the following section). Finally, in the limit $\alpha \to \infty$ it can be shown that the solution of System (11)–(12) converges to the solution of System (9)–(10), the convergence rate being α^{-1}. This can be proved using the analysis developed in [12]. Nevertheless, in our approach α has a physical meaning and, moreover, taking α large leads to ill-conditioning problems.

4. IMPLEMENTATION ASPECTS

4.1. A master–slave algorithm

One important point of the iteration-by-subdomain strategy proposed is that we already had programs that solve the fluid dynamics problem and the structural problem. Then a master/slave algorithm was implemented by developing a third code (the master code) in order to control the iterative process. The MPICH2 library, an implementation of the MPI-2 standard, provides functions for process communications that are used to interchange the data needed to apply boundary conditions on each dedicated (slave) code. Some minor modifications on these codes are needed in order to exchange data with the master. In order to perform a calculation, input data for each subproblem needs to be generated and the master code starts the calculation by starting the slave process (this is only possible under MPI-2 standard). During the calculation, the master code needs to define the boundary conditions to be applied on each subproblem. The situation is illustrated in Figure 3.

4.2. Boundary data interpolation

Another aspect of the implementation that deserves a comment is the interpolation of the boundary conditions to be applied in one subdomain from the results obtained in the other subdomain. For each interface node, this interpolation is performed to find, in the mesh of the other subdomain, the element in which it is located, the so-called host element. The process is illustrated in Figure 4.

The element search strategy used in this study [9] is based on a quad-tree (oct-tree in three dimensions) algorithm. It consists of two steps: the preprocess in which a tree-like structure is built and a process in which the search is performed. In the preprocess, the host computational domain is embedded in a box taking the maximum and minimum nodes coordinates to define its coordinates. This box is then subdivided recursively into four boxes (eight boxes in three dimensions) until each box contains a prescribed (small) number of elements. Once this preprocess has been performed, the process to search the host element of a given point is faster. Given the test point coordinates
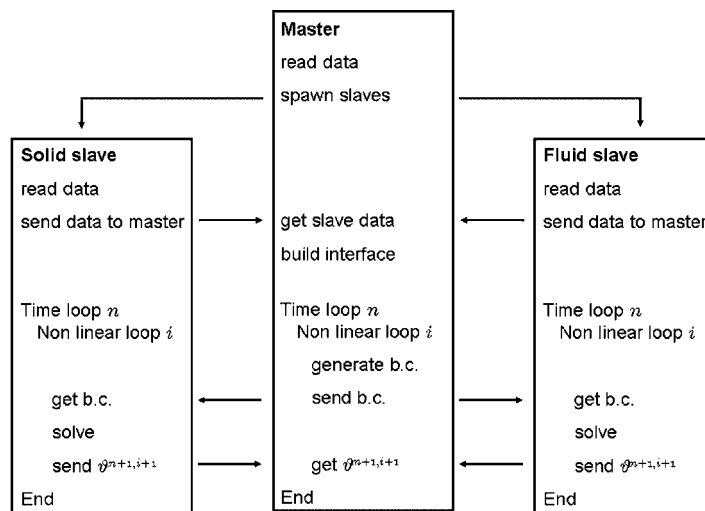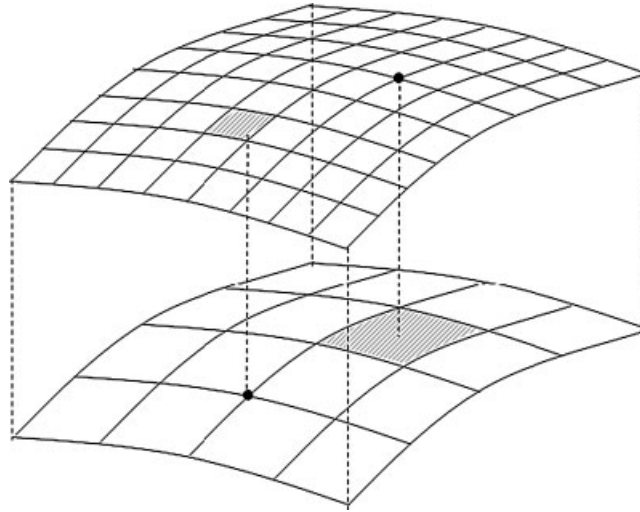

Figure 3. Master–slave implementation.

Figure 4. Boundary data interpolation.

x we recursively locate the boxes it belongs to and we find a small number of elements in which the point must be. Then on each element we perform a local coordinates test. If the coordinates on the parent domain of the standard isoparametric mapping are denoted by ξ, we have

$$\mathbf{x} = \sum_a N^a(\xi)\mathbf{x}^a$$

and starting with **x** we solve this equation for ξ using a Newton–Raphson procedure. The solution permits us to determine whether the point belongs to the element and whether it is the case we already have the shape functions on the host mesh evaluated at that point. They are then used to interpolate the needed boundary data.

5. NUMERICAL EXAMPLES

In this section we present two numerical examples. The first one is a very simple one-dimensional example intended to show the role played by the wall function approach when very thin boundary layers are created. The second example is a practical application of the thermal coupling described in this article.

5.1. A one-dimensional example

Assume that we have two different materials F and S on domains $\Omega_F = [-1, 0]$ and $\Omega_S = [0, 1]$, with conductivities k_F and k_S, respectively, defined by

$$k_F = C \frac{1 - e^{-\gamma}}{1 - e^{-\gamma} + \gamma e^{\gamma x}}$$

$$k_S = C \frac{1 - e^{-\gamma}}{1 - e^{-\gamma} + \gamma e^{-\gamma x}}$$
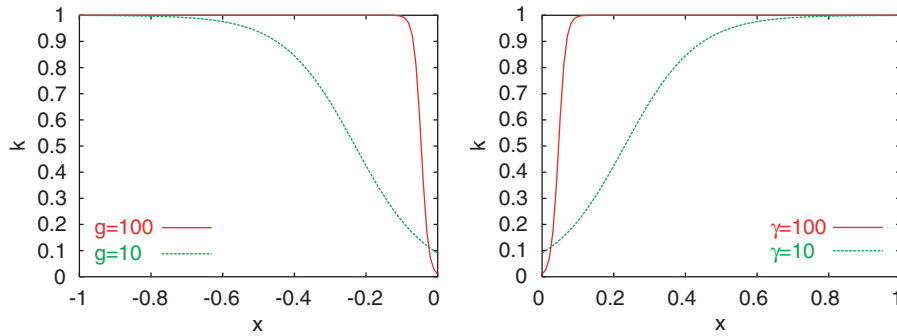
Figure 5. Thermal conductivity.

where C and γ are constants. Both coefficients have a boundary layer near $x=0$ and the constant γ is a measure of the boundary layer width. The coefficients are shown in Figure 5 for $\gamma=10$ and $\gamma=100$ and $C=1$.

The problem can be expressed as

$$-\frac{\mathrm{d}}{\mathrm{d}x}\left(k_{\mathrm{F}}\frac{\mathrm{d}\vartheta}{\mathrm{d}x}\right)=Q_{\mathrm{F}} \quad \text{in } \Omega_{\mathrm{F}}$$

$$-\frac{\mathrm{d}}{\mathrm{d}x}\left(k_{\mathrm{S}}\frac{\mathrm{d}\vartheta}{\mathrm{d}x}\right)=Q_{\mathrm{S}} \quad \text{in } \Omega_{\mathrm{S}}$$

with the transmission conditions

$$-k_{\mathrm{F}}\frac{\mathrm{d}\vartheta}{\mathrm{d}x}=-k_{\mathrm{S}}\frac{\mathrm{d}\vartheta}{\mathrm{d}x} \quad \text{at } x=0$$

$$\vartheta_{\mathrm{F}}(0)=\vartheta_{\mathrm{S}}(0)$$

and the boundary conditions

$$\vartheta_{\mathrm{F}}(-1)=1$$

$$\vartheta_{\mathrm{S}}(1)=0$$

The exact solution to this problem is

$$\vartheta_{\mathrm{F}}(x)=\frac{1}{2}\left(-x+\frac{1-\mathrm{e}^{\gamma x}}{1-\mathrm{e}^{-\gamma}}\right)$$

$$\vartheta_{\mathrm{S}}(x)=\frac{1}{2}\left(-x-\frac{1-\mathrm{e}^{-\gamma x}}{1-\mathrm{e}^{-\gamma}}\right)$$

We have solved this problem in the case of $\gamma=100$ using the first domain decomposition strategy using three different meshes of 10, 20 and 40 elements. The solution is compared with the analytical solution in Figure 6. We have also solved this problem using the second approach using a mesh of 10 elements and the result is compared with the one obtained by the previous method and with the analytical solution in Figure 7. We note that using the first strategy, a better solution can be
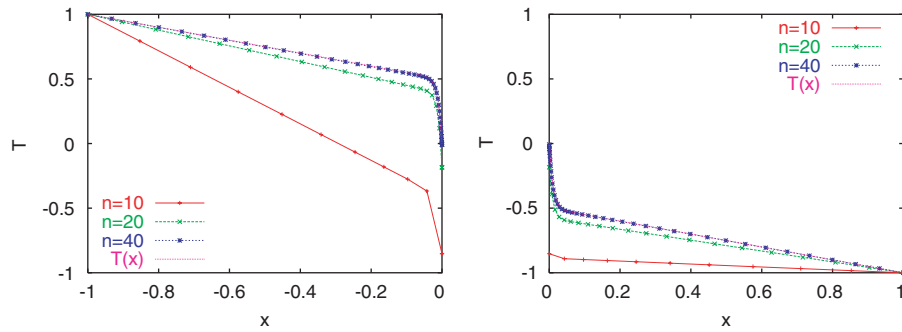
Figure 6. Finite element solution obtained using domain decomposition with two subdomains and meshes of 10, 20 and 40 elements compared with the analytic solution.
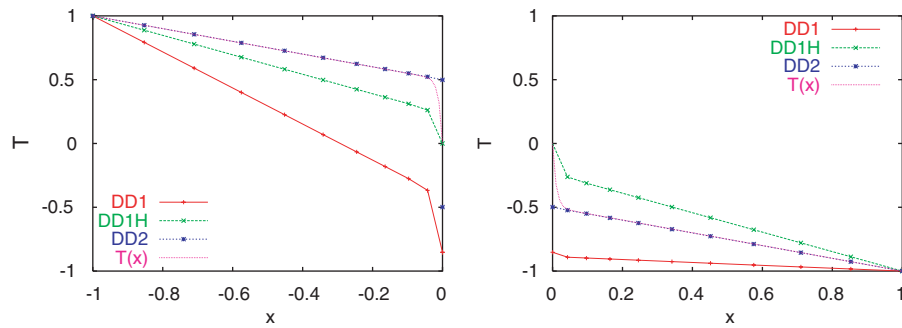

Figure 7. Finite element solution obtained using domain decomposition with two subdomains (DD1), with two subdomains and second-order interpolation of the normal fluxes (DD1H) and with three subdomains (DD2) compared with the analytical solution.

obtained if a second-order approximation of the normal derivatives is made, which implies the need of building an appropriate extrapolation as shown also in Figure 7. This is not a simple task in general domains with unstructured grids.

In any case, it is clear that the second method gives much better results in the case of a coarse discretization. The accuracy of this approach depends on the choice of the coefficient α. The optimal value used here is found noting that, when $\gamma \rightarrow \infty$, the exact solution tends to

$$\vartheta_F(x) = -\tfrac{1}{2}x + \tfrac{1}{2}$$

$$\vartheta_S(x) = -\tfrac{1}{2}x - \tfrac{1}{2}$$

and the conduction coefficients tend to 1 (except at $x = 0$ where both are 0) from where we obtain $\alpha = \tfrac{1}{2}$.

5.2. A fire in a tunnel

A fire is a complex phenomenon whose detailed simulation involves many different aspects that we are not considering in this study. Here we have used a simple model that considers the fire as
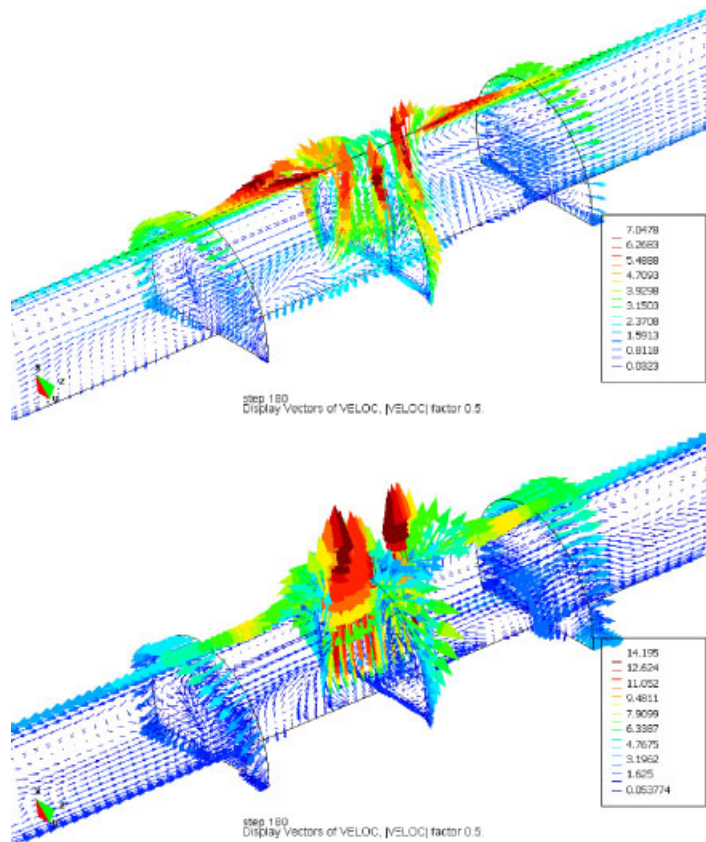
Figure 8. Velocity field at $t=180\,\mathrm{s}$ for $Q=1.25\,\mathrm{MW/m^3}$ (top) and $Q=4.0\,\mathrm{MW/m^3}$ (bottom).

a source of heat, without taking into account the exact reactive mechanism, as this would imply a precise knowledge of the chemical components of the fuel. The heat released during a fire, which is between 1 and 100 MW, is partially dissipated by the flow and partially transported toward the concrete structure where it is finally dissipated. Thus, the heat transfer involves both the behavior of the fluid inside the tunnel and the structural behavior of the concrete and it is therefore necessary to solve a coupled problem.

We solve the problem using the low Mach number approximation to the compressible flow equations. This model takes into account the compressibility of the fluid but removes the acoustic modes [13]. Unlike the Boussinesq approximation, strong temperature and density gradients are allowed. The numerical treatment of the low Mach number equations is described in [14].

The high Reynolds number of the problem implies the need of taking turbulence into account. We do this by introducing a Smagorinsky eddy [15], which is defined as

$$\mu^{\mathrm{t}} = \rho c_s \Delta^2 [\boldsymbol{\varepsilon}'(\mathbf{u}) : \boldsymbol{\varepsilon}'(\mathbf{u})]^{1/2}$$

where c_s is an empirical constant, Δ a characteristic length usually taken as the mesh size and $\boldsymbol{\varepsilon}'(\mathbf{u})$ is the deviatoric part of the rate of deformation tensor. A subgrid thermal conductivity is
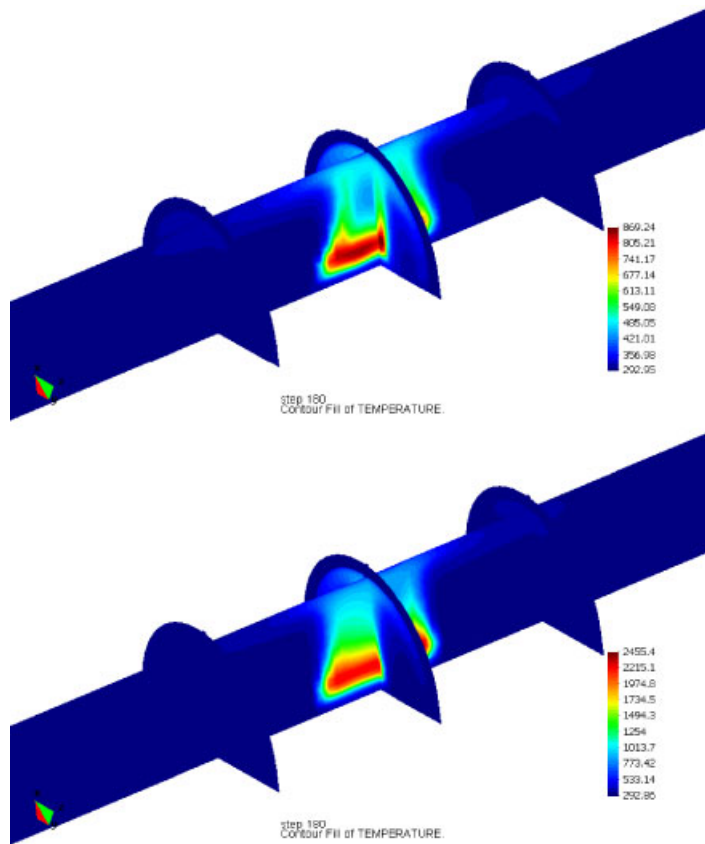
Figure 9. Temperature field at $t = 180\,\mathrm{s}$ for $Q = 1.25\,\mathrm{MW/m}^3$ (top) and $Q = 4.0\,\mathrm{MW/m}^3$ (bottom).

also added. It is defined in terms of the subgrid viscosity as

$$k^{\mathrm{t}} = \frac{\mu^{\mathrm{t}} c_p}{Pr^{\mathrm{t}}}$$

where Pr^{t} is the turbulent Prandtl number, which is assumed to be constant (and taken to be 0.5).

Two simulations were carried out considering heat sources of 10 and 30 MW, which correspond to a small size fire (a car, for example) distributed in a volume of $8\,\mathrm{m}^3$. Based on experimental results, a typical wind in a tunnel in the absence of fire has a velocity of about $0.5\,\mathrm{m/s}$. A preliminary calculation was performed to reproduce the initial state of a wind flowing through the tunnel, which was obtained applying a pressure difference between the tunnel inlet and outlet. On the tunnel walls Neumann boundary conditions based on universal profiles were applied (wall laws). Boundary conditions for temperature were defined to reproduce the real situation as close as possible. On the tunnel walls a Robin-type condition as in (11)–(12) was applied using a convection coefficient suggested by laboratory experiments and the temperature on the concrete walls was fixed. On the entrance and exit of the tunnel, Neumann boundary conditions were considered.
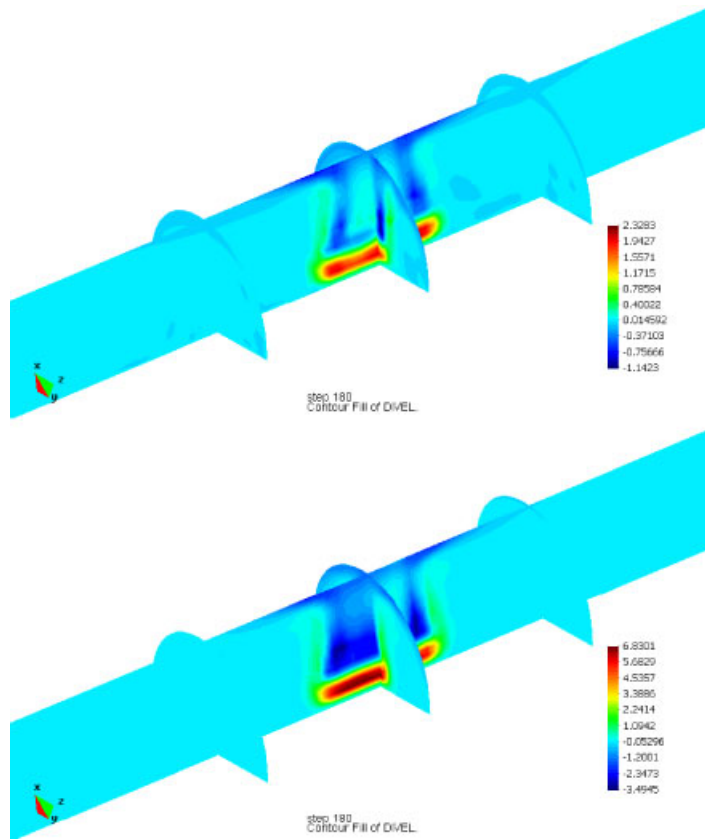
Figure 10. Divergence of the velocity field at $t=180\,\text{s}$ for $Q=1.25\,\text{MW/m}^3$ (top) and $Q=4.0\,\text{MW/m}^3$ (bottom).

The physics of the flow is quite complex and the temporal evolution is chaotic. When the heating starts, strong buoyancy forces determine the formation of a plume and recirculation zones that now, in contrast to the previous example, are fully tridimensional and of complex structure. In Figure 8 the velocity field at 3 min after the starting of the heating is shown and in Figure 9 the corresponding temperature field is shown. Both figures show a detail of the fire zone introducing cutting planes that intersect the fire zone. The heat source generates the plume that can be clearly observed in Figure 8, where an expansion of the flow is also apparent. This expansion is better shown in Figure 10, where contour lines of divergence of the velocity are shown. They have been obtained by projecting velocity gradients on the finite element space.

In both calculations we used a time step $\delta t=1\,\text{s}$. The nonlinear equations describing the flow are solved using two nested loops, an external global loop and internal loops for the momentum equations and for the temperature equation (which is non-linear in the low Mach number case because of the dependence of the density on the temperature). The external loop is also used to account for the domain decomposition coupling. A maximum number of 5 iterations in the external loop were performed with a convergence tolerance of 10^{-3} for the velocity and of 10^{-4} for the

temperature. In most steps, 3 iterations were enough to achieve convergence and only in few steps the temperature residual after 5 iterations was around 0.2×10^{-3} (the velocity residual was always under the prescribed tolerance). The linear system has been solved using a GMRES [16] preconditioned using an ILUT strategy described in [17]. As pointed out in [14], this technique is effective when large time steps are used.

6. CONCLUSIONS

In this article, we have described different aspects related to the numerical approximation of the thermal coupling between a fluid and a solid. Our basic strategy has been to pose the problem in a domain decomposition framework. This has allowed us to propose two alternatives to treat the interface coupling, namely, a classical one considering a perfect thermal contact (continuity of temperatures and heat flux) and another one based on the use of wall functions, which leads to a heat flux proportional to the temperature jump between the fluid and the solid. This surface-convection-like transmission condition depends on a coefficient to which we have given a new expression in terms of the parameters of the wall function approach. When this coefficient increases the perfect thermal contact condition is recovered.

We have also discussed the iteration-by-subdomain strategy we have implemented using a master–slave strategy. Again, the domain decomposition framework turns out to be crucial to formulate this (otherwise standard) iterative strategy.

From the practical point of view, we have found that the algorithmic framework presented here is very handful, easy to implement once the basic dedicated codes are available and, what is more important, robust (in accordance with results known from the literature). An application example of the overall formulation has been presented.

REFERENCES

1. Incropera F, Dewitt D. *Fundamentals of Heat and Mass Transfer* (4th edn). Wiley: New York, 1996.
2. Gawin D, Pesavento F, Schrefler BA. Simulation of damage-permeability coupling in hygro-thermo-mechanical analysis of concrete at high temperature. *Communications in Numerical Methods in Engineering* 2002; **18**: 113–119.
3. Jayatilleke CLV. The influence of Prandtl number and surface roughness on the resistance of laminar sub-layer to momentum and heat transfer. *Progress in Heat Transfer*, vol. 1. Pergamon Press: Oxford, 1969.
4. Codina R, Houzeaux G. Numerical approximation of the heat transfer between domains separated by thin walls. *International Journal for Numerical Methods in Fluids* 2006; **52**:963–986.
5. Codina R. Stabilized finite element approximation of transient incompressible flows using orthogonal subscales. *Computer Methods in Applied Mechanics and Engineering* 2002; **191**(39–40):4295–4321.
6. Codina R, Principe J. Dynamic subscales in the finite element approximation of thermally coupled incompressible flows. *International Journal for Numerical Methods in Fluids* 2007; **54**(6–8):707–730.
7. Codina R, Principe J, Guasch O, Badia S. Time dependent subscales in the stabilized finite element approximation of incompressible flow problems. *Computer Methods in Applied Mechanics and Engineering* 2007; **196**(21–24): 2413–2430.
8. Hughes TJR. Multiscale phenomena, Green's functions, the Dirichlet-to-Neuman formulation, subgrid scale models, bubbles and the origins of stabilized methods. *Computer Methods in Applied Mechanics and Engineering* 1995; **127**:387–401.
9. Houzeaux G. A geometrical domain decomposition method in computational fluid dynamics. *Ph.D. Thesis*, Escola Tècnica Superior d'Enginyers de Camins, Canals i Ports, Universitat Politècnica de Catalunya, Barcelona, 2002.
10. Giles M. Stability analysis of numerical interface conditions in fluid–structure thermal analysis. *International Journal for Numerical Methods in Fluids* 1997; **25**:421–436.

11. Roe B, Haselbacher A, Geubelle P. Stability of fluid–structure thermal simulations on moving grids. *International Journal for Numerical Methods in Fluids* 2007; **54**:1097–1117.
12. Chacón Rebollo T, Chacón Vera E. Study of a non-overlapping domain decomposition method: Poisson and Stokes problems. *Applied Numerical Mathematics* 2004; **48**:169–194.
13. Principe J, Codina R. On the low Mach number and the Boussinesq approximations for low speed flows. *Technical Report*, CIMNE, Publication PI-313, 2008.
14. Principe J, Codina R. A stabilized finite element approximation of low speed thermally coupled flows. *International Journal for Numerical Methods in Heat and Fluid Flow*, to appear.
15. Sagaut P. *Large Eddy Simulation for Incompressible Flows. Scientific Computing*. Springer: Berlin, 2001.
16. Saad Y. *Iterative Methods for Sparse Linear Systems* (1st edn). PWS Publishing Company: Boston, 1996.
17. Saad Y. Ilut: a dual threshold incomplete ILU factorization. *Numerical Linear Algebra with Applications* 1994; **1**:387–402.